ACS APPLIED MATERIALS & INTERFACES

Letter

www.acsami.org

Ultrathin MoS_2 Nanoplates with Rich Active Sites as Highly Efficient Catalyst for Hydrogen Evolution

Ya Yan,[†] BaoYu Xia,[†] Xiaoming Ge,[‡] Zhaolin Liu,[‡] Jing-Yuan Wang,[§] and Xin Wang*[,†]

[†]School of Chemical and Biomedical Engineering, Nanyang Technological University, 62 Nanyang Drive, Singapore 637459, Singapore

[‡]Institute of Materials Research and Engineering (IMRE), Agency of Science, Technology, and Research (A*STAR), 3 Research Link, Singapore 117602, Singapore

[§]Residues and Resource Reclamation Centre, Nanyang Technological University, Singapore 637141, Singapore

Supporting Information

ABSTRACT: Well-defined ultrathin MoS_2 nanoplates are developed by a facile solvent-dependent control route from single-source precursor for the first time. The obtained ultrathin nanoplate with a thickness of ~5 nm features high density of basal edges and abundant unsaturated active S atoms. The multistage growth process is investigated and the formation mechanism is proposed. Ultrathin MoS_2 nanoplates exhibit an excellent activity for hydrogen evolution reaction (HER) with a small onset potential of 0.09 V, a low Tafel slope of 53 mV dec^{-1}, and remarkable stability. This work successfully demonstrates that the introduction of unsaturated active S atoms into ultrathin MoS_2 nanoplates for enhanced electrocatalytic properties is feasible through a facial one-step solvent control method, and that this may open up a potential way for designing more efficient MoS_2-based catalysts for HER.

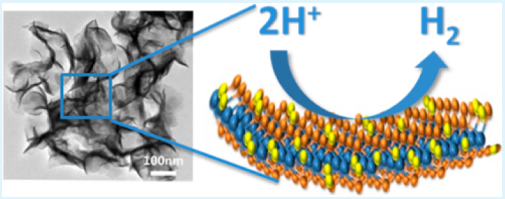

KEYWORDS: *MoS_2 nanoplates, solvent-dependent control, hydrothermal synthesis, unsaturated sulfur atoms, hydrogen evolution reaction, electrocatalyst*

Hydrogen has been vigorously pursued as a promising alternative fuel for traditional fossil fuels,[1] and electrocatalytic hydrogen evolution reaction (HER) is considered to be one of the most important pathways for hydrogen production.[2] Up to now, Pt-group metals have been the most effective electrocatalysts for HER, but the high cost largely prevents their practical application.[3,4] It is therefore important to explore efficient alternatives to the Pt-group metals for hydrogen evolution, preferably based on materials that are cheap and abundant.[5−7]

Over the past few years, molybdenum disulfide (MoS_2) has been extensively studied as the catalysts for HER because of its special structures and electronic properties.[8−15] Recent studies have shown that the HER activity of MoS_2 is highly dependent on the exposed edges.[16−19] Thus, designing MoS_2 nanosheets with more edge sites is one effective strategy to enhance activity, and a lot of effort has been focused on achieving this.[20−25] Furthermore, the S content in MoS_2 also plays an important role in HER process, as indicated by the traditional hydrodesulphurization (HDS) process.[26,27] The unsaturated sulfur atoms on the surface of MoS_2 materials can engage the discharge reaction and easily form S−H bonds, thus leading to hydrogen formation eventually. For example, Hu's group reported that amorphous MoS_3 particles, which contain catalytically active S_2^{2-} ligands, show superior catalytic activity towards HER.[12] This result was further validated by Li's group recently,[28] where the higher HER efficiency of the MoS_x materials is related to the presence of bridging S_2^{2-} or apical S^{2-} in amorphous states. However, the amorphous MoS_2 structure may lead to relatively poor electrochemical stability in the acid electrolyte and most of the reported methods involve complicated manipulation. Therefore, it is still a big challenge to prepare MoS_2 nanocatalysts with high HER activity and good stability by a facile method.

Herein, a well-defined MoS_2 nanocatalysts with abundant active unsaturated S atoms is developed by a novel and facile solvent-dependent method. This highly tunable synthesis offers three advantages: (i) the ultrathin MoS_2 nanoplates are rich with basal edges, thus increasing the density of active sites; (ii) the active S ligands can be introduced into the ultrathin platelike MoS_2 structure, leading to a more efficient MoS_2 catalyst for HER than simple MoS_2; and (iii) the direct growth of the ultrathin MoS_2 nanoplates by a solvent dependent method with single source precursor is very facile and controllable. The obtained MoS_2 nanoplates have been characterized by various techniques. As expected, the ultrathin MoS_2 nanoplates show outstanding catalytic performance for HER. Moreover, the growth mechanism of ultrathin MoS_2 nanoplates is also first explained.

The ultrathin MoS_2 nanoplates are obtained by solvothermal treating $(NH_4)_2MoS_4$ in the mixture of *N, N*-Dimethylforma-

Received: October 31, 2013
Accepted: December 3, 2013
Published: December 3, 2013

mide (DMF) and H_2O (V_{DMF}:V_{H2O} = 2:1) at 210 °C for 18 h. The field-emission scanning electron microscopy (FESEM) image (Figure 1a) clearly shows the well-defined platelike

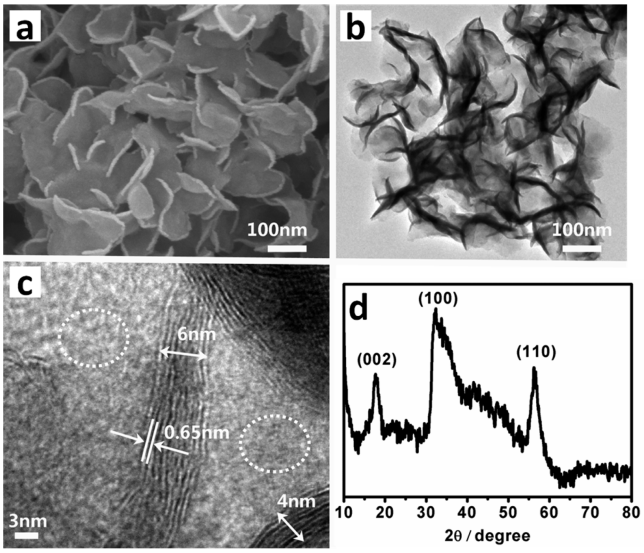

Figure 1. (a) FESEM, (b) TEM, (c) high-resolution (HR) TEM images, and (d) XRD pattern of ultrathin MoS_2 nanoplates.

morphology of the MoS_2, where the lateral size of the plates is in the range of 200−300 nm. Figure1b is a representative transmission electron microscopy (TEM) image, showing good agreement with SEM observation (Figure 1a). The light contrast in various areas of the TEM image indicates the thin two-dimensional (2D) nature of the platelike nanostructures. Besides, dense interconnected ripples and corrugations can also be observed, suggesting the basal-edge-rich feature of the ultrathin MoS_2 nanoplates. The high-resolution (HR)TEM image (Figure1c) of the curled edge shows the MoS_2 plates are composed of 7−10 layers (4−6 nm) with an interlayer spacing of 0.65 nm, further verifying the ultrathin nature of the MoS_2 plates. Importantly, the absence of the interplanar lattice (001) observed from the HRTEM image as indicated by the white circle, suggests that the nanoplate material is low crystallinity. This is further confirmed by the X-ray diffraction (XRD) pattern (Figure1d), where all the diffraction peaks match the hexagonal phase of MoS_2 (2*H*-MoS_2), but the weak (00*l*) diffraction illustrates the low crystallinity. Especially, the low intensity of the (002) diffraction of the *c* axis suggests the MoS_2 plates consist of a few layers of nanosheets, whereas the slight (002) peak shift could be attributed to the distortion of lattice in the as-prepared MoS_2 nanoplates. Finally, the energy-dispersive X-ray (EDX) mapping images (Figure S1, see the Supporting Information) confirm the homogeneous distribution of Mo and S elements across the whole nanoplates.

The chemical states of Mo and S in the ultrathin nanoplates are analyzed by X-ray photoelectron spectroscopy (XPS) technique. It can be observed that two characteristic peaks arising from 229.0 and 232.2 eV are attributed to the Mo $3d_{5/2}$ and $3d_{3/2}$ binding energies for a Mo (IV) oxidation state (Figure 2a), while the corresponding peaks for the S $2p_{3/2}$ and $2p_{1/2}$ orbitals of divalent sulfide ions (S^{2-}) are observed at 161.8 and 163.1 eV (Figure 2b).[29] In addition to the XPS peaks for the pure MoS_2 structure, another set of small peaks for S and Mo are also presented (Figure 2a, b). The observation of

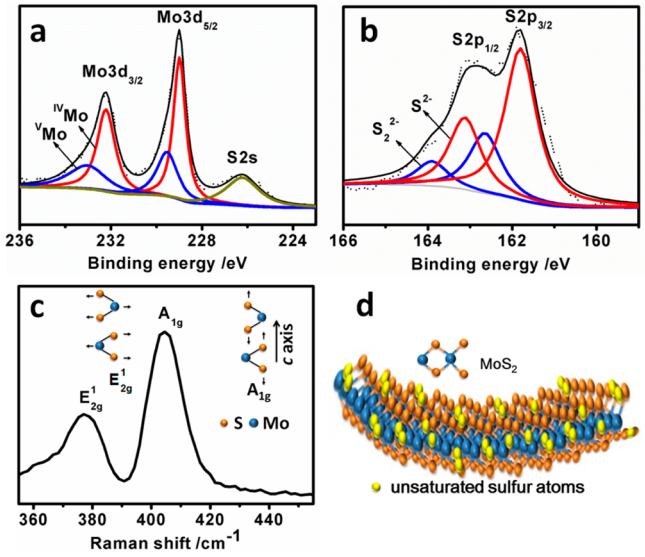

Figure 2. XPS spectra of (a) Mo 3d and (b) S 2p, (c) Raman spectrum for ultrathin MoS_2 nanoplates. Inset of c shows the atomic displacement of the E^1_{2g} and A_{1g} vibrational modes in bulk MoS_2. (d) illustration for the ultrathin MoS_2 nanoplates with unsaturated S atoms.

Mo $3d_{5/2}$ and $3d_{3/2}$ peaks at lower binding energies suggests the presence of Mo (V),[28] whereas the peaks for S $2p_{3/2}$ and $2p_{1/2}$ at 162.6 and 163.9 eV indicate the presence of bridging S_2^{2-} or apical S^{2-}, which result from the unsaturated S atoms, as indicated in panels a and b in Figure 2.[30] To further verify the XPS results, we performed Raman spectra to have further detailed insight on the structure of the nanoplates. As shown in Figure 2c, the characteristic Raman shifts at 377 and 404 cm^{-1} expected for the E^1_{2g} and A_{1g} vibrational modes of hexagonal MoS_2 are clearly observed (inset of Figure 2c), respectively. Moreover, compared with the Raman spectrum of calcined MoS_2 nanoplates (see Figure S2 in the Supporting Information), the relatively larger peak width and weaker intensity of E^1_{2g} peak of the ultrathin MoS_2 nanoplates indicate that the crystal structure of MoS_2 is not perfect and in-layer disorder or defects exist between the Mo and S atoms. Meanwhile, the lower intensity of E^1_{2g} peak compared with A_{1g} peak further reveals the basal-edge-rich feature of the ultrathin MoS_2 nanoplates,[31] in good agreement with TEM observation (Figure 1b). On the basis of the above analysis, we accordingly suspect that certain amount of "defect sites" may exist on the surface of the nanoplates, which in turn provide sites for the formation of unsaturated S atoms. Thus, a model of MoS_2 nanoplate with unsaturated S atoms on the surface is proposed and schemed in Figure 2d, where those unsaturated S atoms exist either on the basal edges or the defect sites of the basal planes. As suggested by the atomic composition and binding energies measured from XPS and the low crystalline structure observed from TEM and XRD, the as-prepared nanoplate material is predominately composed of low-crystalline MoS_2 with unsaturated sulfur atoms.

It has been discovered that the ratio of DMF and H_2O plays an essential role in determining the final morphology of the ultrathin MoS_2 nanoplates. When only DMF is used, the as-formed thick nanoplates aggregate and assemble into large particles, which is denoted as thick MoS_2 nanoplate assemblies (Figure S3a, see the Supporting Information). With the addition of H_2O into the reaction solution, the aggregation

phenomenon becomes less severe and the samples exhibit plate morphologies (Figure S3b, see the Supporting Information). With the further increase in the volume ratio of H_2O to DMF, the as-formed plates become thinner such that eventually the plates curled up and shielded its basal edges, as shown in Figure S3c–e (see the Supporting Information). Thin conglutinated nanosheets are formed with the presence of H_2O only (Figure S3f, see the Supporting Information). These results obtained in our work might illustrate that DMF plays a role for the formation of the platelike shape, whereas the amount of H_2O in the mixture could adjust and control the thickness of the nanoplates. More importantly, H_2O would also take part in the dispersion and crystallinity for the final MoS_2 nanostructures (Figure 1 and Figure S3, see the Supporting Information). A suitable concentration of $(NH_4)_2MoS_4$ in the starting solvent (V_{DMF}:V_{H2O} = 2:1) would result in MoS_2 nanoplate with uniform dispersion (Figure S4, see the Supporting Information). With the further increase of $(NH_4)_2MoS_4$ amount gradually from 20 to 40 mg, the morphology of the products evolves from well-defined nanoplates to nanoplate assemblies followed by flowerlike nanostructure, and eventually to large nanoflowers. The formation of the nanoflower morphology at high $(NH_4)_2MoS_4$ concentration might be due to the self-assembly of the nanoplate building blocks to minimize the total surface energy.

The morphology evolution of MoS_2 nanoplates during the solvothermal process is further examined by FESEM techniques. In the first stage for 40 min, large amounts of MoS_2 nanoparticles are formed with a size ~10 nm (Figure 3a).

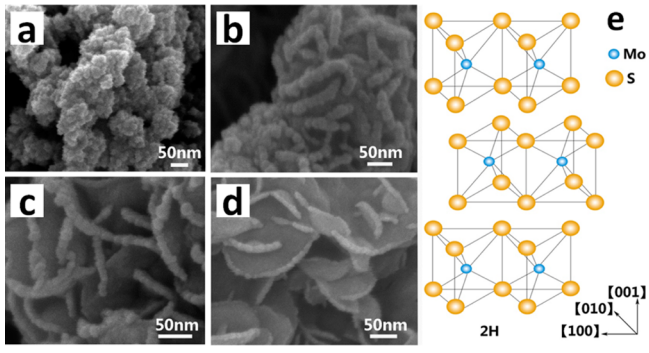

Figure 3. FESEM images of the products obtained at different growth stages: (a) 40 min, (b) 60 min, (c) 1.5 h, and (d) 2 h. (e) Schematic illustration of the 2*H*-type structure of MoS_2.

Subsequently, these nanoparticles spontaneously aggregate into spherical cores of size ~200 nm with sawtooth-structured protuberances growing from the core (Figure 3b). After reaction for 1.5 h, the randomly aligned nanopetals originating from the sawtooth-structured protuberances are observed (Figure 3c), which are so large that the originally spherical core is no longer evident. As the reaction continues (Figure 3d), the inner amorphous spherical core diminishes gradually and the growth occurs on randomly aligned nanopetals as those petals grow into well-defined interconnected nanoplates with smooth basal plan and edges. Reactions for longer time are also found to form similar plate-like nanostructures, suggesting they are the final thermodynamically stable products. These observations agree with previous reports of the growth mechanism involving a multistage growth process.[32−34] Thus, the growth and morphology of the platelike MoS_2 nanostructures may be understood as follows. The particles initially formed are amorphous and thus adopt a spherical shape. The surface of the spheres acts as nucleation sites for the formation of sawtooth-structured protuberances consisting of small crystalline particles of MoS_2. As the reaction proceeds, it is energetically more favorable for the crystalline MoS_2 protuberances to grow, where they evolve from small nanopetals to well-defined interconnected MoS_2 plates with the protuberances on the surface of these spheres providing high-energy sites for crystal growth. The platelike 2D shape of the protuberances and interconnected lamellars originate from the layered structure of MoS_2, which grows preferentially along the [100] and [010] directions compared to the longer [001] direction as shown in Figure 3e.

Featured by rich basal edges and active unsaturated sulfur atoms, the ultrathin MoS_2 nanoplates are expected to show better HER performance than conventional MoS_2 nanoplates. Figure 4a shows the polarization curves for the various catalysts

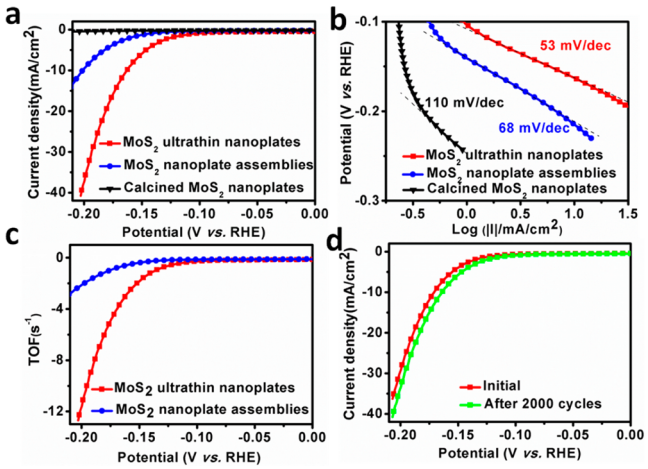

Figure 4. (a) Polarization curves, (b) corresponding Tafel plots and (c) calculated turnover frequencies of various samples. (d) Stability test for the ultrathin MoS_2 nanoplates.

(with correction for ohmic potential drop (*i*R) losses, see Figures S5 and S6 in the Supporting Information). For comparison purpose, electrochemical measurements are also conducted on thick MoS_2 nanoplate assembly with less edge sites and calcined ultrathin MoS_2 nanoplates with high crystallinity (Figure S7, see the Supporting Information). The ultrathin MoS_2 nanoplates exhibits excellent activity for the HER with a low onset potential of approximately −0.09 V (determined from the semi-log plot as shown in Figure S10, see the Supporting Information), which surpasses the activities for the rest both MoS_2 samples. To obtain further insight into the HER on ultrathin MoS_2 nanoplates, Tafel plots of various catalysts are investigated (Figure 4b). The resulting Tafel slope of the ultrathin MoS_2 nanoplates is 53 mV dec^{-1}, which matches with several earlier reports for the MoS_2 catalysts.[25,35] By contrast, this value is significantly lower than that of the calcined MoS_2 nanoplates. Maintaining similar morphology (Figure S7a, see the Supporting Information), the calcined sample shows much higher crystallinity as confirmed by XRD results (Figure S7b, see the Supporting Information). XPS spectra exhibits only a single doublet for Mo 3d and S 2p (Figure S7c, d, see the Supporting Information), suggesting the lack of bridging S_2^{2-} or apical S^{2-}. These observations indicate

dx.doi.org/10.1021/am404843b | ACS Appl. Mater. Interfaces 2013, 5, 12794−12798

that the ultrathin MoS_2 nanoplates prepared are featured with more active sites steming from the coordinately unsatureated sites and surfur atoms, which are suspected to be the reasons why the ulttathin MoS_2 nanoplates are more active than MoS_2 with higher crystallinity. Moreover, compared to the thick MoS_2 nanoplate assemblies in terms of Tafel slope, the comparatively smaller value for MoS_2 ultrathin nanoplates may be explained by the fact that more accessible catalytically active edges are created because of the unique ultrathin morphology, as described below.

To directly investigate the effect of the additional active edges brought in by the ultrathin shape, the turnover frequency (TOF) is then calculated over the ultrathin MoS_2 nanoplates and the thick MoS_2 nanoplate assemblies by quantifying the active sites through electrochemical approach (Figure S8, see the Supporting Information).[36] The calculated active edge sites of ultrathin MoS_2 nanoplates is larger than that of thick MoS_2 nanoplate assemblies, giving the direct evidence of the enhanced active edge sites brought in by the ultrathin nature of the nanoplates and the abundant exposed S active atoms. This view could further be supported by the larger Brunauer-Emmett-Teller (BET) surface area of the ultrathin MoS_2 nanoplates (56 cm^2 g^{-1}) in comparison to the thick MoS_2 nanoplate assembly (28 cm^2 g^{-1}) (Figure S9, see the Supporting Information), since higher surface area of the ultrathin nanoplate morphology can result in a higher density of accessible reactive sites. Figure 4c shows the polarization curves normallized by the active sites, which are expressed in term of TOF. The calculated TOF number per active site for the MoS_2 ultrathin nanoplates reaches 0.15 s^{-1} at η = 0 mV, which is higher than the value (0.10 s^{-1}) for thick MoS_2 nanoplate assemblies, suggesting the improved intrinsic activity of the active sites due to the unsaturated active S atoms existed on the surface of ultrathin nanoplates. Hence, the high hydrogen-evolving activity of MoS_2 ultrathin nanoplates can be attributed to the combined presence of active unsaturated S ligands and additional edge sites generated in this ultrathin nanoplate morphology.

Finally, the catalytic stability of the ultrathin MoS_2 nanoplates catalyst towards the HER is assessed. Figure 4d displays the polarization curves of ultrathin MoS_2 nanoplate before and after 2000 cycles. The negligible decay of the cathodic currents indicates the good stability of the ultrathin MoS_2 nanoplates in a long-term electrochemical process. Previous reports for active MoS_x nanoparticls demonstrated a high S/Mo atomic ratio in the range of 2.5−3.0 and were basically amorphous.[28,30] Therefore, poor stability of these MoS_x materials is expected during the HER under acidic condition. In contrast, the analysis of the Mo (3d) and S (2p) peak intensities for our material yields an S/Mo ratio of ∼2.10, suggesting that the structure is not pure MoS_2 but close to MoS_2 while retaining abundant active S atom. It is worth noting that the stability performance obtained in our work is better than that of the amorphous MoS_2 reported previously, which may suggest that the crystalline MoS_2 in the structure could stabilize the catalytically active S−S bonds, thus leading to a low solubility of MoS_2 nanoplates in the acidic solution.[12,35]

In conclusion, we report a facile solvent-dependent control route for the synthesis of ultrathin MoS_2 nanoplates with unsaturated active S atoms from single source precursor. The growth mechanism of ultrathin MoS_2 nanoplates is proposed. The existence of unsaturated active sulfur ligands and edge-rich ultrathin layers results in the exposure of additional catalytically-active sites, leading to outstanding catalytic performance for the HER. This study successfully demonstrates that introducing unsaturated sulfur ligands to ultrathin MoS_2 nanoplates is feasible by a facile solvent-dependent control route and this may open up a potential pathway for designing more efficient MoS_2-related catalyst for HER.

■ ASSOCIATED CONTENT

Supporting Information

Details of the experimental method and obtained data. This material is available free of charge via the Internet at http://pubs.acs.org/.

■ AUTHOR INFORMATION

Corresponding Author

*E-mail: WangXin@ntu.edu.sg. Fax: +65 67947553.

Notes

The authors declare no competing financial interest.

■ ACKNOWLEDGMENTS

We acknowledge financial support from the academic research fund AcRF tier 1 (M4011020 RG8/12) Ministry of Education, Singapore, and competitive research program (2009 NRF-CRP 001-032), National Research Foundation, Singapore. The support by the Singapore National Research Foundation under its Campus for Research Excellence And Technological Enterprise (CREATE) programme is also acknowledged.

■ REFERENCES

(1) Armor, J. N. *Catal. Lett.* **2005**, *101*, 131−135.
(2) Turner, J. A. *Science* **2004**, *305*, 972−974.
(3) Casado-Rivera, E.; Volpe, D. J.; Alden, L.; Lind, C.; Downie, C.; Vázquez-Alvarez, T.; Angelo, A. C. D.; DiSalvo, F. J.; Abruña, H. D. *J. Am. Chem. Soc.* **2004**, *126*, 4043−4049.
(4) Greeley, J.; Jaramillo, T. F.; Bonde, J.; Chorkendorff, I.; Norskov, J. K. *Nat. Mater.* **2006**, *5*, 909−913.
(5) Chen, W.-F.; Sasaki, K.; Ma, C.; Frenkel, A. I.; Marinkovic, N.; Muckerman, J. T.; Zhu, Y.; Adzic, R. R. *Angew. Chem., Int. Ed.* **2012**, *51*, 6131−6135.
(6) Kuang, Q.; Yang, S. *ACS Appl. Mater. Interfaces* **2013**, *5*, 3683−3690.
(7) Xu, H.; Ouyang, S.; Li, P.; Kako, T.; Ye, J. *ACS Appl. Mater. Interfaces* **2013**, *5*, 1348−1354.
(8) Zeng, Z.; Yin, Z.; Huang, X.; Li, H.; He, Q.; Lu, G.; Boey, F.; Zhang, H. *Angew. Chem. Int. Ed.* **2011**, *50*, 11093−11097.
(9) Xiang, Q.; Yu, J.; Jaroniec, M. *J. Am. Chem. Soc.* **2012**, *134*, 6575−6578.
(10) Balendhran, S.; Walia, S.; Nili, H.; Ou, J. Z.; Zhuiykov, S.; Kaner, R. B.; Sriram, S.; Bhaskaran, M.; Kalantar-zadeh, K. *Adv. Funct. Mater.* **2013**, *23*, 3952−3970.
(11) Chen, P.; Xiao, T.-Y.; Li, H.-H.; Yang, J.-J.; Wang, Z.; Yao, H.-B.; Yu, S.-H. *ACS Nano* **2011**, *6*, 712−719.
(12) Benck, J. D.; Chen, Z. B.; Kuritzky, L. Y.; Forman, A. J.; Jaramillo, T. F. *ACS Catal.* **2012**, *2*, 1916−1923.
(13) Wang, T.; Liu, L.; Zhu, Z.; Papakonstantinou, P.; Hu, J.; Liu, H.; Li, M. *Energy Environ. Sci.* **2013**, *6*, 625−633.
(14) Wang, M.; Li, G.; Xu, H.; Qian, Y.; Yang, J. *ACS Appl. Mater. Interfaces* **2013**, *5*, 1003−1008.
(15) Zhang, C.; Wang, Z.; Guo, Z.; Lou, X. W. *ACS Appl. Mater. Interfaces* **2012**, *4*, 3765−3768.
(16) Hinnemann, B.; Moses, P. G.; Bonde, J.; Jørgensen, K. P.; Nielsen, J. H.; Horch, S.; Chorkendorff, I.; Nørskov, J. K. *J. Am. Chem. Soc.* **2005**, *127*, 5308−5309.
(17) Jaramillo, T. F.; Jørgensen, K. P.; Bonde, J.; Nielsen, J. H.; Horch, S.; Chorkendorff, I. *Science* **2007**, *317*, 100−102.

(18) Karunadasa, H. I.; Montalvo, E.; Sun, Y.; Majda, M.; Long, J. R.; Chang, C. J. *Science* **2012**, *335*, 698−702.
(19) Yan, Y.; Xia, B.; Qi, X.; Wang, H.; Xu, R.; Wang, J.-Y.; Zhang, H.; Wang, X. *Chem. Commun.* **2013**, *49*, 4884−4886.
(20) Jaramillo, T. F.; Bonde, J.; Zhang, J.; Ooi, B.-L.; Andersson, K.; Ulstrup, J.; Chorkendorff, I. *J. Phys. Chem. C* **2008**, *112*, 17492−17498.
(21) Chen, Z.; Cummins, D.; Reinecke, B. N.; Clark, E.; Sunkara, M. K.; Jaramillo, T. F. *Nano Lett.* **2011**, *11*, 4168−4175.
(22) Kibsgaard, J.; Chen, Z.; Reinecke, B. N.; Jaramillo, T. F. *Nat. Mater.* **2012**, *11*, 963−969.
(23) Laursen, A. B.; Kegnaes, S.; Dahl, S.; Chorkendorff, I. *Energy Environ. Sci.* **2012**, *5*, 5577−5591.
(24) Liao, L.; Zhu, J.; Bian, X.; Zhu, L.; Scanlon, M. D.; Girault, H. H.; Liu, B. *Adv. Funct. Mater.* **2013**.
(25) Xie, J.; Zhang, H.; Li, S.; Wang, R.; Sun, X.; Zhou, M.; Zhou, J.; Lou, X. W.; Xie, Y. *Adv. Mater.* **2013**, DOI: 10.1002/adma.201302685.
(26) Vrinat, M.; Breysse, M.; Geantet, C.; Ramirez, J.; Massoth, F. *Catal. Lett.* **1994**, *26*, 25−35.
(27) McCain, M. N.; He, B.; Sanati, J.; Wang, Q. J.; Marks, T. J. *Chem. Mater.* **2008**, *20*, 5438−5443.
(28) Chang, Y.-H.; Lin, C.-T.; Chen, T.-Y.; Hsu, C.-L.; Lee, Y.-H.; Zhang, W.; Wei, K.-H.; Li, L.-J. *Adv. Mater.* **2013**, *25*, 756−760.
(29) Weber, T.; Muijsers, J. C.; van Wolput, J. H. M. C.; Verhagen, C. P. J.; Niemantsverdriet, J. W. *J. Phys. Chem.* **1996**, *100*, 14144−14150.
(30) Vrubel, H.; Merki, D.; Hu, X. *Energy Environ. Sci.* **2012**, *5*, 6136−6144.
(31) Kong, D.; Wang, H.; Cha, J. J.; Pasta, M.; Koski, K. J.; Yao, J.; Cui, Y. *Nano Lett.* **2013**, *13*, 1341−1347.
(32) Burda, C.; Chen, X.; Narayanan, R.; El-Sayed, M. A. *Chem. Rev.* **2005**, *105*, 1025−1102.
(33) Cheng, Y.; Wang, Y.; Zheng, Y.; Qin, Y. *J. Phys. Chem. B* **2005**, *109*, 11548−11551.
(34) Enyashin, A. N.; Bar-Sadan, M.; Sloan, J.; Houben, L.; Seifert, G. *Chem. Mater.* **2009**, *21*, 5627−5636.
(35) Merki, D.; Fierro, S.; Vrubel, H.; Hu, X. L. *Chem. Sci.* **2011**, *2*, 1262−1267.
(36) Yan, Y.; Ge, X.; Liu, Z.; Wang, J.-Y.; Lee, J.-M.; Wang, X. *Nanoscale* **2013**, *5*, 7768−7771.